frontiers | Frontiers in Environmental Science

TYPE Original Research
PUBLISHED 07 June 2024
DOI 10.3389/fenvs.2024.1429684

OPEN ACCESS

EDITED BY
Xudong Peng,
Guizhou University, China

REVIEWED BY
Youjin Yan,
Nanjing Forestry University, China
Yusong Deng,
Guangxi University, China

*CORRESPONDENCE
Le-Xing You,
leoxyou@zjnu.edu.cn
Jin-Shi Lin,
jslin@fafu.edu.cn

RECEIVED 08 May 2024
ACCEPTED 21 May 2024
PUBLISHED 07 June 2024

CITATION
Jiang L, Chen J, You L-X, Jiang F-S, Zhang Y, Lin J-S and Huang Y-H (2024), Free iron oxides modulate the surface properties of Benggang soil on Southern China: insights into erosive mechanisms.
Front. Environ. Sci. 12:1429684.
doi: 10.3389/fenvs.2024.1429684

Free iron oxides modulate the surface properties of Benggang soil on Southern China: insights into erosive mechanisms

Ling Jiang[1], Jie Chen[1], Le-Xing You[2]*, Fang-Shi Jiang[1], Yue Zhang[1], Jin-Shi Lin[1]* and Yan-He Huang[1]

[1]College of Resources and Environment, Fujian Agriculture and Forestry University, Fuzhou, China, [2]College of Geography and Environmental Sciences, Zhejiang Normal University, Jinhua, China

Benggang, an erosional phenomenon located in southern China, exhibits distinctive characteristics that can have profound ecological and agricultural consequences as well as pose risks to human life. Previous investigations have primarily focused on elucidating the relationships between the physical and chemical attributes of soils collected from Benggang. However, the precise role of free iron oxides in the surface properties of Benggang soil and its contribution to the formation of Benggang remains largely unexplored. In this study, we aim to investigate the role of free iron oxides in Benggang soil by removing them and subsequently introducing goethite to evaluate their impact on the soil's surface properties. Our results reveal a decrease in the surface charge density of soil colloidal particles with increasing soil depth. Specifically, the uppermost red soil layer exhibits the highest value, followed by the sandy soil and the lowermost clastic layer. Upon removing free iron oxide, we documented reductions of 44.28% (red soil), 20.62% (sandy soil), and 8.70% (clastic layer) in the surface charge density of colloidal particles. The red soil layer presented an over 18-fold increase compared to the initial linear shrinkage, followed by the sandy soil and clastic layer. Notably, the addition of goethite to the iron oxide-free soil layers resulted in the recovery of approximately 81.93%, 121.13%, and 104.35% of the initial surface charge density, respectively. Moreover, significant changes in volume shrinkage were observed, with approximately 97.54% (red soil), 94.75% (sandy soil), and 89.72% (clastic layer) of the initial values being influenced. These findings underscore the substantial influence of free iron oxide on the physicochemical properties of Benggang soil and contribute to a comprehensive understanding of the erosive mechanisms underlying Benggang formation.

KEYWORDS

Benggang, free iron oxide, shrinkage, surface charge density, surface potential

1 Introduction

Benggang is a unique erosional phenomenon in southern China that forms where sloping soil- and stone-rich horizons become fragmented, collapse, and are further scoured away due to the combined actions of water and gravity (Xu, 1996). Benggang formation can severely impact agricultural production and cause the loss of human life, as well as can hinder the development of the social economy in affected regions (Zhong et al., 2013).

Therefore, it is important to comprehensively understand the occurrence and the development of Benggang over time to prevent their formation in the future and/or control their influence when they occur.

Many studies have focused on the macroscopic erosive driving forces that contribute to Benggang formation, and it is widely believed that this type of collapse is influenced by multiple factors, including geomorphology (Chaplot, 2013), vegetation cover (Gyssels et al., 2005; Wang et al., 2014), water flow (Xu and Zeng, 1992; Jiang et al., 2014; Lin et al., 2017), and soil characteristics (Six et al., 2004). Extensive research has been conducted on the physicochemical properties of soil in Benggang, encompassing dry density, water content, clay mineral composition and content (Chen et al., 2018; Wang et al., 2018; Wei et al., 2018; Xia et al., 2019; 2021; Zhang et al., 2022). During periods of rainfall, soil swelling is induced as a result of a rapid influx of water content. Subsequent to the rainfall event, gradual evaporation of soil moisture occurs, leading to soil shrinkage as the water content diminishes. The repetitive cycles of wet and dry conditions exacerbate the development of cracks initiated by soil swelling and shrinkage, ultimately expediting soil erosion processes (Zhang et al., 2023). However, the specific triggers for Benggang formation remain unclear due to the multitude of influential factors.

Charged soils, which contained particles with negative and/or positive charges, are widespread in nature. Phyllosilicates typically exhibit a net negative surface charge under normal pH conditions, whereas iron oxides carry a net positive surface charge (Yu, 1997; Qafoku et al., 2004). Previous studies have demonstrated that the presence of iron oxide can induce a shift in the zeta potential of soil towards positive values (Hou et al., 2007; Jiang et al., 2010; Wang et al., 2013), resulting in corresponding alterations in physicochemical properties such as the linear shrinkage ratio and cation-exchange capacity (Zhang and Kong, 2014). Importantly, the soil surrounding Benggang contains a substantial amount of iron oxide and kaolinite, distinguishing it from other charged soils like purple soil and loessal soil. When this charged soil is dispersed in water, electrical double layers form on both kaolinite and iron oxides. These oppositely charged particles interact with each other by overlapping diffuse layers of electric double layers (Qafoku and Sumner, 2002; Qafoku et al., 2004), thereby altering the surface charge density and subsequently impacting the stability of the soil aggregates (Gao et al., 2019). However, the influence of iron oxides on the surface properties of Benggang soil and their contribution to the formation of Benggang remains largely unexplored despite extensive research in this area.

Moreover, the soil collected in and around Benggang exhibits a distinct layering pattern based on depth, consisting of red soil, sandy soil, and clastic layers. The presence of varying mineralogical compositions within these horizons can lead to significant modifications in their physicochemical properties (Chen et al., 2018). Furthermore, a comparison between Benggang soil and soil collected prior to its formation reveals a decrease in iron oxide concentrations within the red soil layers following the erosive event, while the opposite trend is observed in the sandy soil and clastic layers (Huang et al., 2019). This raises a pivotal question regarding the role of iron oxide content as the primary factor triggering Benggang formation.

To address this issue, we conducted soil sampling in the vicinity of a Benggang in southern China, removing free iron oxide and subsequently introducing goethite to examine the resulting changes in soil properties. Through the analysis of surface charge density and shrinkage characteristics of the red soil, sandy soil, and clastic layers, we aim to elucidate the role of free iron oxides in influencing the surface properties of each soil type and their impact on Benggang formation.

2 Study area

The undisturbed soil samples used in this study were collected from Benggang located at Yangkeng Village in Longmen Town, Fujian Province, China, (118° 05′E, 24° 57′N), which corresponds to the same site as documented in Huang et al. (2019). A multi-point sampling approach was adopted (Figure 1), wherein three soil samples were collected within a defined area of each layer (approximately 0.5 hm^2) to create a composite sample representative of that particular horizon.

3 Material and methods

3.1 Soil physicochemical properties and pretreatment

The bulk density, pH (using a solution-to-soil ratio of 5:1), cation-exchange capacity, and mineralogical compositions of the red soil (Soil-A_1), sandy soil (Soil-A_2), and clastic layers (Soil-A_3) in the undisturbed soil samples were measured in accordance with the methodology outlined in our previous study (Zhang et al., 2023). Subsequently, the undisturbed soil samples were naturally air-dried and ground to achieve a particle size smaller than 2 mm. Approximately 50 g of each soil sample was mixed with 25 mL of a 30% H_2O_2 solution in a 500-mL beaker, which was then subjected to heating at 75°C while simultaneously being mechanically agitated until no bubbles were observed. This process effectively removed all organic matter present in the soil samples. All reagents utilized in the experiment were of analytical grade, and ultrapure water sourced from a Milli-Q Labo apparatus (Nihon Millipore Ltd.) was used for the preparation of solutions. Unless specifically noted, all experiments in this study were replicated three times and all results are expressed as means ± standard deviation (n = 3).

3.2 Removal and addition of iron

The removal of free iron oxides from the undisturbed soil samples in each layer (labeled as Soil-B_1, Soil-B_2, and Soil-B_3) was conducted through a series of meticulous steps (Wu et al., 2017; Chen et al., 2018). Initially, a beaker containing pretreated soil was subjected to a stepwise addition of 40 mL of a sodium citrate solution (0.3 M), 5 mL of a sodium bicarbonate solution (1 M), and 2 g of sodium dithionite. This process was carried out at a temperature of 80°C and repeated until the color of the soil transitioned from red to gray. Subsequently, the gray soil was subjected to three consecutive rinses with deionized water through centrifugation at 4,000 rpm for 20 min per rinse. The resulting precipitate was then freeze-dried for a duration of 10 h

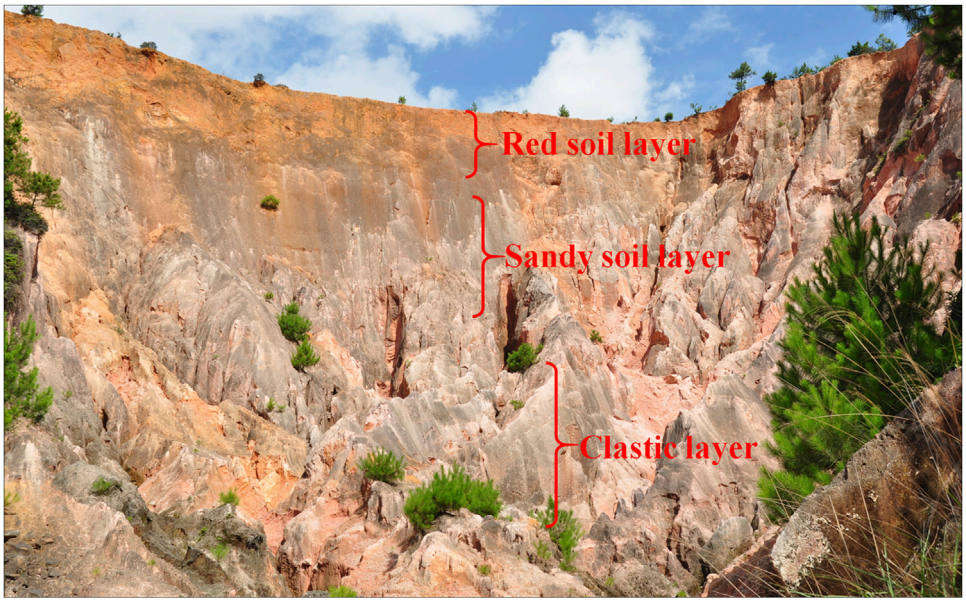

FIGURE 1
Photograph of a typical Benggang at Yangkeng Village in Longmen Town, Fujian Province, China. The layered soil structure and associated sampling sites are labeled.

and subsequently sieved using a 2-mm sieve. The concentration of free iron oxides present in the supernatant was determined using phenanthroline colorimetry.

The introduction of iron into Soil-B was accomplished through the following procedure (Ma et al., 2007). Firstly, the initial moisture content of Soil-B was measured using conventional drying techniques. Subsequently, 53.94 g, 45.75 g, and 35.83 g of goethite was separately added to 1,000 g of the Soil-B_1, Soil-B_2, and Soil-B_3 layers, respectively. These goethite additions were thoroughly mixed with deionized water until homogeneity was achieved, ensuring the absence of any agglomerations. The resulting prepared soils, designated as Soil-C_1, Soil-C_2, and Soil-C_3, were sealed overnight and subsequently placed in an uncovered plastic box to cultivate at room temperature for a period of 1 month. The water content of each soil sample during this process was maintained at 20% ± 1%. Finally, each soil sample was air-dried and passed through a 2-mm sieve.

3.3 Soil shrinkage ratio test

Each pretreated soil sample was diluted with deionized water to achieve a bulk water content of 15% ± 1%. The mixture was thoroughly mixed until homogenized and subsequently sealed, allowing it to sit undisturbed overnight. After that, a ring-knife sample (diameter, 61.8 mm; height, 20 mm) was prepared from this soil using conventional geotechnical test methods. This process was repeated three times for each soil sample to ensure reliability. To determine the linear shrinkage rate, a soil constrictor (TKA-SSY-1, Nanjing Teco Technology Co., LTD, China) equipped with a data acquisition box (TKA-Dai-8D) and data acquisition and processing software V2.1 was employed. After performing these experiments, the height, diameter, and weight of each soil sample was determined to obtain their water content and longitudinal and transverse shrinkage rates.

3.4 Soil surface property

3.4.1 Collection of soil colloidal particles

Each pretreated soil sample (i.e., Soil-A, Soil-B, and Soil-C) was subjected to a sequential addition of approximately 300 mL of deionized water and 10 mL of a 5% sodium metaphosphate solution. The mixture was then placed in a high-speed mixer and stirred for a duration of 10 min at a speed of 500 rpm. The well-stirred soil liquid was subsequently transferred into a 1-L measuring cylinder and further stirred 30 times using a stirring rod. After allowing the suspension to settle for a period of 20 h, the uppermost 7 cm of the suspension within the measuring cylinder was carefully collected. This collected suspension was then subjected to centrifugation and freeze-drying processes to obtain soil colloidal particles with a size of less than 1,000 nm. The crystalline components of all the soil colloidal particles were analyzed using an automated Rigaku Utimal X-ray diffractometer (XRD) equipped with Cu kα radiation. The XRD analysis was performed under the following operating conditions: 40 kV × 40 mA and a 2θ degree angle ranging from 10° to 90° at a scan rate of 4° min^{-1}.

3.4.2 Determination of surface charge density

The surface charge properties of the soil colloids were determined following the combined method of Li et al. (2011), which involved multiple steps. Firstly, 10 g of the colloidal particles from each soil sample (as previously described) were carefully placed in a 500-mL centrifuge bottle, ensuring a soil-to-liquid ratio of 1:5. Subsequently, 50 mL of 0.1 M HCL solution was added to the bottle, and the mixture was subjected to centrifugation for a duration of

12 h. After that, the supernatant was discarded, and this procedure was repeated three times, after which it was finally freeze-dried. Next, 2 g of the freeze-dried soil colloid particles were transferred into another 500-mL centrifuge bottle and were oscillated for 12 h during the addition of 15 mL of 0.02 M $Ca(OH)_2$ solution. Following this, another 24 h period of oscillation was carried out, during which 15 mL of 0.02 M NaOH was added. The pH value of the mixture was adjusted to a range of 6.0–8.0 after the oscillation. This process continued for at least 12 h until the pH reached a neutral value. Finally, the mixed solution was subjected to centrifugation at a speed of 4,000 rpm to obtain the supernatant. The concentrations of Ca^{2+} and Na^+ in the supernatant were measured by atomic absorption spectrometry (PerkinElmer, PinAAcle900F, United States of America) and flame photometry (FP640, Shanghai Precision and Scientific Instrument Co., Ltd., China). The surface charge density (σ_0) and surface potential (φ_0) in the mixed system were calculated as follows (Li et al., 2011):

$$\sigma_0 = \frac{(N_{Na^+} + 2N_{Ca^{2+}}) \times F \times 10^{-5}}{S}$$

$$S = \frac{\kappa N_{Na^+}}{mC^0_{Ca}} e^{\frac{\beta_{Na} F \varphi_0}{2RT}}$$

$$\varphi_0 = \frac{2RT}{(\beta_{Ca} - \beta_{Na})F} ln \frac{C_{Ca^0} N_{Na^+}}{C_{Na^0} N_{Ca^{2+}}}$$

$$\beta_{Ca} = 2 - \beta_{Na} = -0.0213\, ln\, I^{0.5} + 1.2331$$

$$\kappa = \sqrt{\frac{8\pi F^2 C^0}{\varepsilon RT}}$$

Where C_{Na^0}, C_{Ca^0}, N_{Na^+}, and $N_{Ca^{2+}}$ are the bulk concentrations and the adsorbing capacities of Na^+ and Ca^{2+}, respectively. β_{Ca} and β_{Na} are the relative charge coefficients of Na^+ and Ca^{2+}, respectively. $I^{0.5}$ is the square root of the ionic strength in the bulk solution. R, T, F, and S represent the gas constant, absolute temperature (Kelvin), Faraday constant, and the specific surface area of charged soil particles, respectively. κ, m, and ε denote the Debye–Hückel parameter, the modification factor ($m = 0.5259\, ln(\frac{C_{Na^0}}{C_{Ca^0}}) + 1.992$) and the dielectric constant of water, respectively.

3.5 Statistical analysis

Data analysis was conducted using IBM SPSS statistics, employing the least significant difference approach. Specifically, One-way ANOVA with Dunnett's T3 method was utilized for analyzing the shrinkage rate following the removal and subsequent introduction of iron, while the Pearson method was applied to assess the correlation between the soil swelling rate of different soil layers and the shear plane thickness of colloidal particles.

4 Results

4.1 Physical properties of the pretreated soils

The undisturbed soil comprised three distinct types: red soil (Soil-A_1), sandy soil (Soil-A_2), and clastic layers (Soil-A_3). These soils exhibited bulk densities of 1.31, 1.32, and 1.49 g·cm^{-3}, respectively. The pH values of these soils, measured using a solution to soil ratio of 5:1, was determined to be 5.06, 4.82, and 4.65 g·cm^{-3}, respectively. The cation-exchange capacity for Soil-A_1, Soil-A_2, and Soil-A_3 was found to be 8.25, 3.33, and 2.67 cmol·kg^{-1}, respectively. The content of free iron oxide in the red soli was the highest, with a value of 48.57 g·kg^{-1}, followed by the sand soil with 41.19 g·kg^{-1} and debris layers with 32.26 g·kg^{-1}.

Figure 2 displayed the XRD spectra of soil colloidal particles extracted from the pretreated soils. These spectra were carefully compared to relevant references (Chen et al., 2018; Huang et al., 2019) for identification of crystalline types within soil before and after the addition of goethite. The XRD analysis revealed that the red soil and sandy soil layers within Soil-A demonstrated distinct reflection peaks at 6.1°, 8.8°, 12.3°, 18.2°, 24.8°, and 26.6° (Figure 2A), indicating the presence of hydroxy-interlayered vermiculite, illite and kaolinite. Similarly, the clastic layers exhibited characteristic diffraction peaks of illite and kaolinite at 8.8°, 12.3°, 24.8° and 26.6°. These findings align well with previous studies (Huang et al., 2019; Zhang et al., 2023). Notably, the removal of free iron oxide from the undisturbed soil had negligible impact on these XRD reflection peaks, as shown in Figure 2B. Upon the introduction of goethite to Soil-B, the reflection peaks at 8.8°, 12.3°, 18.2°, 24.8°, and 26.6° remained unaltered, while the peak at 6.1° was not observed due to its significantly lower relative intensity (Figure 2C). A new distinct characteristic diffraction peak emerged at 28.4° in Soil-C (Figure 2C). Through a comparative analysis of these spectra with those of Soil-A, Soil-B, and the standard data JCPDS 29-0713 and 54-0489, it was determined that the emergence of this new peak could be attributed to the presence of Fe_2O_3, which originated from the introduction of goethite.

4.2 Shrinkage characteristics

As shown in Figure 3A, it could be observed that the clastic layer of the undisturbed soil exhibited the highest linear shrinkage rate (0.40%) during the 96-h measurement period, while the sandy and red soil layers in the undisturbed soil experienced minimal changes, with linear shrinkage rates of 0.32% and 0.13%, respectively. Upon the removal of free iron oxides (Figure 3B), the red soil layer (Soil-B_1) demonstrated the most pronounced linear shrinkage rate, reaching a magnitude of 2.38%. This value presented an over 18-fold increase compared to the initial linear shrinkage. Subsequently, the sandy soil layer and the clastic layer followed suit with linear shrinkage rates of 1.15% and 0.42%, respectively. Furthermore, upon the addition of goethite (Figure 3C), the corresponding red soil layer (Soil-C_1), sand soil layer (Soil-C_2), and clastic (Soil-C_3) layers experienced a degree of restoration, resulting in linear shrinkage rates of 1.65%, 0.85% and 0.45%, respectively. We also conducted a significance test on the linear shrinkage rate following the removal and subsequent addition of iron. As a result, significant changes ($\rho < 0.05$) were noted in the red soil and sandy soil; however, no statistically significant change ($\rho > 0.05$) was observed in the clastic layer.

To further evaluate the impact of free iron oxide on the soils, we followed the established guidelines outlined by Mishra et al. (2020), wherein we calculated the volume shrinkage of ring-knife samples subsequent to shrinkage. As illustrated in Figure 4, the red soil layer exhibited the most substantial disparity in volume after the removal of free iron oxide, with a magnitude of 14,592.19 mm^3. The sandy

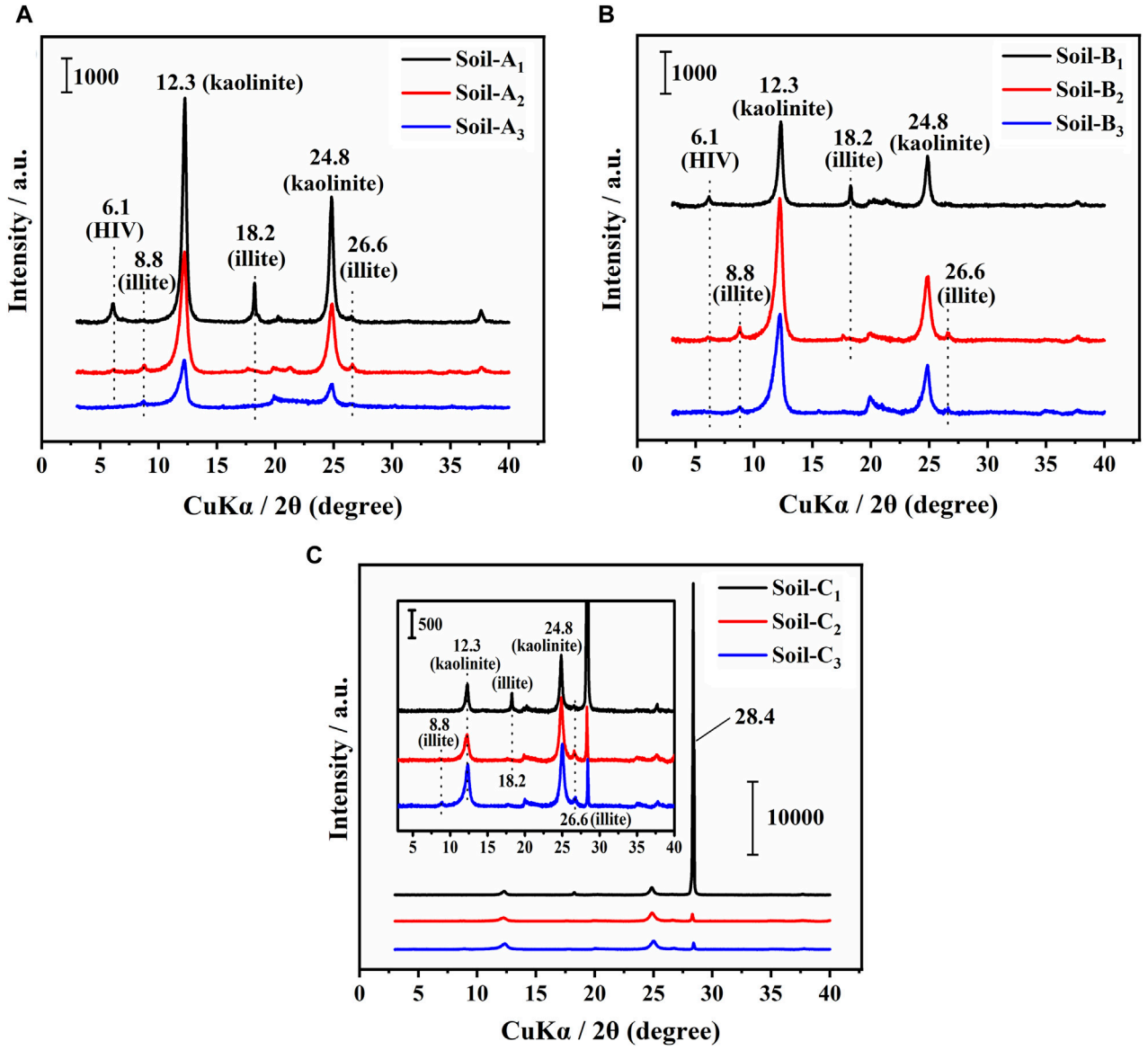

FIGURE 2
XRD spectra of soil colloidal particles collected from **(A)** undisturbed soil (Soil-A), **(B)** undisturbed soil without free iron oxides (Soil-B), and **(C)** Soil-B with the addition of goethite (Soil-C). The inset in part **(C)** shows an enlargement of the spectra. Numbers are as follows: 1, red soil layers; 2, sandy soil layers; 3, clastic soil layers. HIV: hydroxy-interlayered vermiculite.

soil layer followed suit with a volume difference of 9,343.09 mm^3, while the clastic layer displayed a comparatively minor volume difference of 550.14 mm^3. Subsequently, in the case of Soil-B, when subjected to goethite cultivation, the volume shrinkages of Soil-C_1, Soil-C_2, and Soil-C_3 were determined to be approximately 97.54%, 94.75%, and 89.72% of the initial value of the corresponding undisturbed soil layers, respectively.

4.3 Surface charge density of the pretreated soil colloidal particles

Table 1 demonstrated that the surface potential of soil colloidal particles from each soil layer ranged from −67.77 ± 4.73 mV to −82.01 ± 4.88 mV, which correlated with findings reported for purple soil (Ding et al., 2015). For the undisturbed soil (Soil-A), the surface potential of red soil colloidal particles (Soil-A_1) was more negative at −79.78 ± 3.55 mV compared to sandy soil (Soil-A_2) at −76.52 ± 2.03 mV and the clastic (Soil-A_3) layer at −70.94 ± 3.84 mV. Similarly, the calculated surface charge density of the red soil colloidal particles (Soil-A_1, 3.32 ± 0.33 × 10^{-2} C·m^{-2}) was considerably higher than for the sandy soil (Soil-A_2, 1.94 ± 0.04 C·m^{-2}) and the clastic (Soil-A_3, 1.61 ± 0.31 C·m^{-2}) layer. Upon removing free iron oxides from the undisturbed soil, the cation-exchange capacity for the red soil, sandy soil, and clastic layer changed by 6% each. Most importantly, reductions of 44.28%, 20.62%, and 8.70% were observed in the surface charge density of colloidal particles collected from the red soil (Soil-B_1), sandy soil

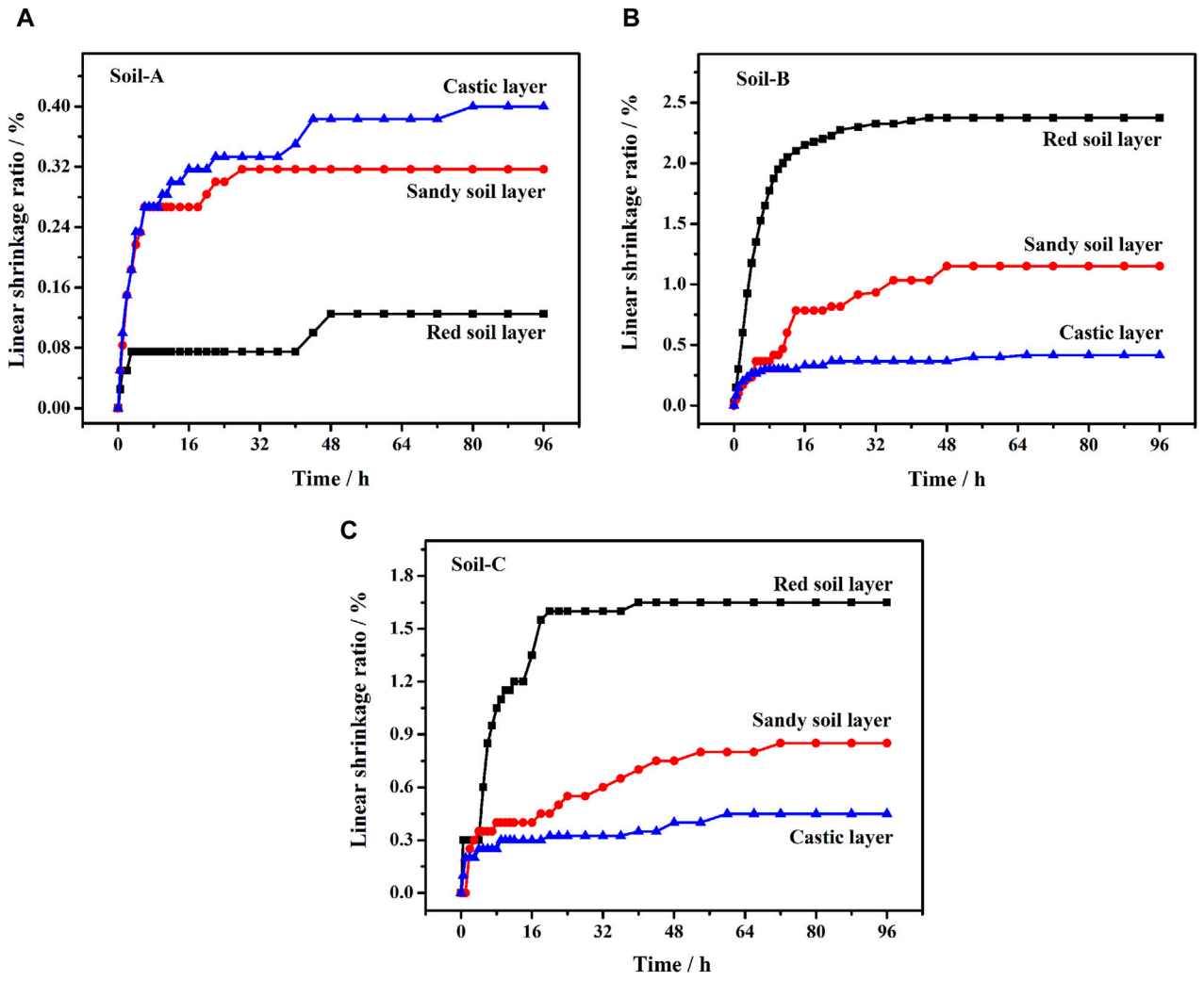

FIGURE 3
Linear shrinkage ratio of **(A)** undisturbed soil (Soil-A), **(B)** undisturbed soil without free iron oxides (Soil-B), and **(C)** Soil-B with the addition of goethite (Soil-C).

(Soil-B_2), and clastic layer (Soil-B_3), respectively. Subsequently, upon the introduction of goethite into Soil-B, the initial surface charge density increased by approximately 81.93% (Soil-C_1), 121.13% (Soil-C_2), and 104.35% (Soil-C_3) in comparison to the corresponding layers in the undisturbed soil. Furthermore, the surface potential of the red soil experienced a reduction after the removal of free iron oxides, which was subsequently reversed by the addition of goethite. In contrast, opposite trend was observed for sandy soil. Notably, the surface potential of the clastic layer did not show significant influence through this process.

4.4 Pearson correlation between the content of free iron oxide and soil properties

Table 2 presented the Pearson correlations between the content of free iron oxide and various soil properties. The analysis revealed that the content of free iron oxide in all soil layer exhibited a consistently low negative correlation with the linear shrinkage rate, and no significant change in this relationship was observed. Furthermore, the analysis indicated the absence of any significant positive correlation between the content of free iron oxide and volume shrinkage. Additionally, no statistically significant correlation was estimated between the content of free iron oxide and surface potential. In contrast, the content of free iron oxide demonstrated moderate and statistically significant negative correlations with the specific surface area of charged soil particles ($\rho < 0.05$), and surface charge density ($\rho < 0.05$).

5 Discussion

Previous studies have extensively documented the profound influence of clay minerals on the physicochemical and surface properties of soil (Hou et al., 2007; Jiang et al., 2010; Wang et al., 2013). In this study, we conducted a designed experiment to investigate the role of free iron oxide in Benggang soil layers, including red, sandy and detritus soil layers. To achieve this, we employed a rigorous

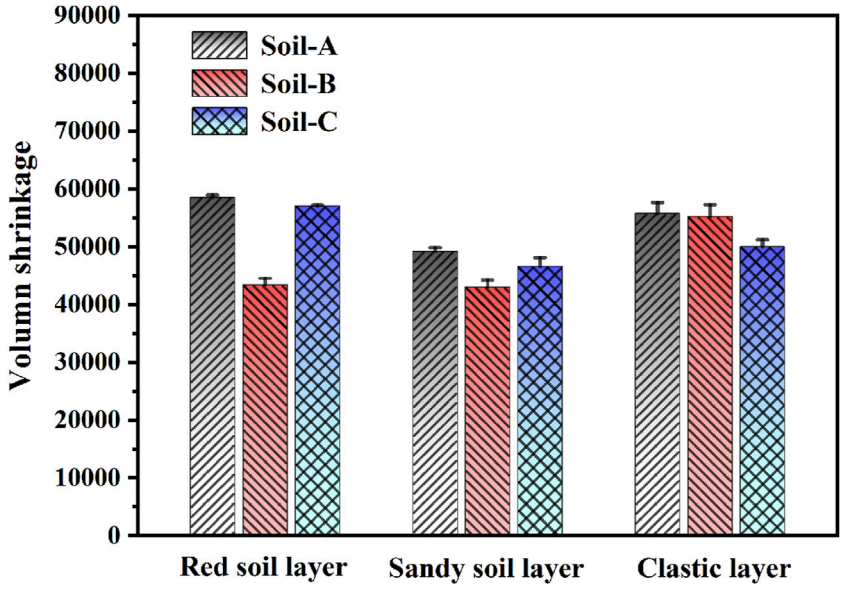

FIGURE 4
Volume shrinkage of undisturbed soil (Soil-A), undisturbed soil without free iron oxides (Soil-B), and Soil-B with the addition of goethite (Soil-C).

TABLE 1 Surface properties of colloidal particles for all pretreated soils.

Soil type	C_{Na+} (10^{-3} M)	C_{Ca2+} (10^{-3} M)	Adsorbing capacity (10^{-2} mol kg^{-1})		S (10^3 m^2 kg^{-1})	φ_0 (mV)	σ_0 (10^{-2} C m^{-2})
			Na^+	Ca^{2+}			
A_1	3.62 ± 0.13	1.28 ± 0.15	3.67 ± 0.01	3.91 ± 0.02	33.33 ± 3.76	−79.78 ± 3.55	3.32 ± 0.33
B_1	1.93 ± 0.21	0.57 ± 0.06	3.84 ± 0.02	3.97 ± 0.01	61.38 ± 15.06	−82.01 ± 4.88	1.85 ± 0.34
C_1	3.14 ± 0.08	1.23 ± 0.09	3.71 ± 0.08	3.90 ± 0.07	41.16 ± 2.94	−76.87 ± 2.33	2.72 ± 0.17
A_2	2.26 ± 0.13	0.87 ± 0.13	3.80 ± 0.01	3.94 ± 0.01	57.88 ± 1.53	−76.52 ± 2.03	1.94 ± 0.04
B_2	1.92 ± 0.07	0.87 ± 0.14	3.84 ± 0.01	3.94 ± 0.01	73.51 ± 8.49	−72.7 ± 4.73	1.54 ± 0.21
C_2	2.57 ± 0.90	0.87 ± 0.10	3.77 ± 0.09	3.94 ± 0.01	47.87 ± 2.29	−79.57 ± 2.76	2.35 ± 0.11
A_3	2.08 ± 0.21	1.02 ± 0.07	3.82 ± 0.02	3.93 ± 0.01	70.01 ± 10.61	−70.94 ± 3.84	1.61 ± 0.31
B_3	2.03 ± 0.07	1.14 ± 0.22	3.83 ± 0.01	3.91 ± 0.02	76.43 ± 10.42	−67.77 ± 4.73	1.47 ± 0.17
C_3	2.28 ± 0.06	1.21 ± 0.10	3.80 ± 0.08	3.91 ± 0.02	65.63 ± 6.82	−69.30 ± 3.97	1.68 ± 0.18

A, undisturbed soil (Soil-A); B, undisturbed soil without free iron oxides (Soil-B); C, Soil-B, with the addition of goethite (Soil-C); 1, red soil layers; 2, sandy soil layers; and 3, clastic soil layers.

TABLE 2 Pearson correlation between the presence of free iron oxide and soil properties.

	Parameter	S (10^3 m^2 kg^{-1})	φ_0 (mV)	σ_0 (10^{-2} C m^{-2})	Linear shrinkage rate (%)	Volume shrinkage
Fe ($g{\cdot}kg^{-1}$)	Pearson correlation	−0.771*	−0.279	−0.702*	−0.34	0.502
	Two-tailed test	0.015	0.468	0.035	0.370	0.168

Asterisk indicates significant values at the 0.05 level (two-tailed).

methodology, which involved the systematic removal of free iron oxide from all soil layers and the subsequent introduction of goethite into the respective soil layers. Our analysis of the XRD spectra revealed that the removal of free iron oxide did not exert a significant influence on the presence of characteristic reflection peaks. However, upon the addition of goethite, a distinct change manifested in the XRD spectra, specifically the emergence of a well-defined diffraction peak at 28.4° (Figure 2). It is crucial to note that this peak was attributed to Fe_2O_3 rather than

goethite. This distinction arises from the fact that goethite in the soil, with the passage of 1 month of cultivation, underwent a process of remodeling after and was ultimately transformed into iron oxide.

The shrinkage characteristic of soil is a fundamental parameter that plays a crucial role in assessing its mechanical properties. Upon removing free iron oxide from Benggang soil, we observed a remarkable increase in the initial linear shrinkage of the red soil and sandy soil layers, with magnitudes exceeding 18-fold and 3.5-fold, respectively. However, no significant change occurred in the clastic layer (Figure 3B). In contrast, upon the introduction of goethite, a substantial decrease in the linear shrinkage rates was observed. Specifically, the red and sandy soil layers exhibited reductions of over 12-fold and 2.6-fold, respectively (Figure 3C). These phenomena could be attributed to the fact that soil physical properties, including soil cohesion, were directly influenced the presence of free iron oxide (Zhang and Kong, 2014). The rapid escalation of soil shrinkage rate directly contributed to the instability of the soil structure, potentially leading to soil erosion. In particular, loose subsoil, such as sandy or detritus soil layer, with low Fe-oxide contents disintegrated first after rainfall, followed by the collapse of the structurally stable red soil with high Fe-oxide contents, ultimately resulting in soil erosion. When goethite was introduced into the corresponding soil layers in the absence of free iron oxide, a significant volume shrinkage of approximately 97.54%, 94.75%, and 89.72% of the initial value was observed in the undisturbed red, sandy and detritus soil layers, respectively. These results clearly established a direct correlation between the presence of free iron oxide content in the soil and the magnitude of shrinkage it underwent.

The removal of free iron oxide and the introduction of goethite possess the inherent capabilities to induce alterations in both the surface charge density and surface potential, which, in turn, have the potential to exert a profound influence on the overall stability of a soil aggregate (Gao et al., 2019). Our measurements of the surface charge density of soil colloidal particles collected from the undisturbed Benggang soil revealed a range of values, ranging from −67.77 ± 4.73 mV to −82.01 ± 4.88 mV (Table 1). These values were consistent with previous findings of −82.8 ± 5.2 mV reported for acidic purple soil with a pH of 4.65 (Ding et al., 2015). However, they slightly differed from the values of −82.79 ± 4.73, −63.45 ± 5.39, and −90.55 ± 13.73 mV obtained in our previous study (Zhang et al., 2023), possibly due to variations in soil physicochemical properties, such as pH value. The removal of free iron oxide (Soil-B) resulted in a decrease in the surface charge density with increasing soil depths, indicating that the presence of free iron oxides had the most significant influence on the surface charge density. Subsequently, upon adding goethite into the corresponding soil layers in the absence of free iron oxide (Soil-C), the surface charge densities reached approximately 81.93%, 121.13%, and 104.35% of the initial surface charge density. Obviously, the impact of free iron oxide varied among soil layers, consistent with the observed variation in soil shrinkage mentioned earlier. The relationships between the content of free iron oxide and soil properties (Table 2), including surface potential, surface charge density and shrinkage, further confirmed the aforementioned results. Nevertheless, the absence of a substantial correlation between shrinkage and free iron oxide content, might be attributed to the fact that alterations in the levels of free iron oxides directly affect soil cohesion, thereby indirectly influencing soil swelling and shrinkage dynamics.

6 Conclusion

Our experimental results show that the surface charge density of undisturbed soil colloidal particles in a Benggang decreases with depth: specifically, the red soil layer has the highest surface charge density, and the debris (clastic) layer has the lowest surface charge density. After the removal of free iron oxide from each layer, this effect did not change, and reductions of 44.28%, 20.62%, and 8.70% were determined for surface charge density of the colloidal particles for red soil, sandy soil, and clastic layers, respectively. After the addition of goethite, the soil colloidal particles recovered approximately 81.93%, 121.13%, and 104.35% of their initial surface charge density, respectively. Furthermore, free iron oxide has an impact on soil shrinkage characteristics, which is especially pronounced for the red soil layer. Approximately 97.54% (red soil), 94.75% (sandy soil), and 89.72% (clastic layer) of the initial volume shrinkage can be achieved by the addition of goethite into the iron oxide-free soil layers, respectively. These results indicate that free iron oxide has the maximum influence on the surface charge density of soil colloidal particles and shrinkage characteristics in red soil layers, followed by sandy soil and clastic layers.

Data availability statement

The raw data supporting the conclusion of this article will be made available by the authors, without undue reservation.

Author contributions

LJ: Investigation, Methodology, Writing–original draft. JC: Investigation, Visualization, Writing–original draft. L-XY: Conceptualization, Data curation, Writing–review and editing. F-SJ: Formal Analysis, Writing–review and editing. YZ: Formal Analysis, Writing–review and editing. J-SL: Conceptualization, Resources, Writing–review and editing. Y-HH: Funding acquisition, Project administration, Supervision, Writing–review and editing.

Funding

The author(s) declare that financial support was received for the research, authorship, and/or publication of this article. This work was supported by the National Natural Science Foundation of China (grant number 41571272), Water Conservancy Science and Technology Project of Fujian Province (KJG21009A), and Modern Agricultural-Industrial Collaborative Innovation Center of Anxi County (KMD18003A).

Conflict of interest

The authors declare that the research was conducted in the absence of any commercial or financial relationships that could be construed as a potential conflict of interest.

Publisher's note

References

Chaplot, V. (2013). Impact of terrain attributes, parent material and soil types on gully erosion. *Geomorphology* 186, 1–11. doi:10.1016/j.geomorph.2012.10.031

Chen, J., Zhou, M., Lin, J., Jiang, F., Huang, B., Xu, T., et al. (2018). Comparison of soil physicochemical properties and mineralogical compositions between noncollapsible soils and collapsed gullies. *Geoderma* 317, 56–66. doi:10.1016/j.geoderma.2017.12.006

Ding, W., Zhu, Q., Wang, L., Luo, Y., Li, Q., Zhu, H., et al. (2015). Calculation of thickness of shear plane in diffuse double layer of constant charge soil colloid in single electrolyte system. *Acta Pedol. Sin.* 52, 859–868. doi:10.11766/trxb201409060453

Gao, X., Li, S., Liu, X., Hu, F., Tian, R., and Li, H. (2019). The effects of NO3- and Cl-on negatively charged clay aggregation. *Soil till. Res.* 186, 242–248. doi:10.1016/j.still.2018.10.025

Gyssels, G., Poesen, J., Bochet, E., and Li, Y. (2005). Impact of plant roots on the resistance of soils to erosion by water: a review. *Prog. Phys. Geog.* 29, 189–217. doi:10.1191/0309133305pp443ra

Hou, T., Xu, R. K., Tiwari, D., and Zhao, A. Z. (2007). Interaction between electrical double layers of soil colloids and Fe/Al oxides in suspensions. *J. Colloid Interf. Sci.* 310, 670–674. doi:10.1016/j.jcis.2007.02.035

Huang, B., Qiu, M., Lin, J., Chen, J., Jiang, F., Wang, M. K., et al. (2019). Correlation between shear strength and soil physicochemical properties of different weathering profiles of the non-eroded and collapsing gully soils in southern China. *J. Soil. Sediment.* 19, 3832–3846. doi:10.1007/s11368-019-02313-7

Jiang, F. S., Huang, Y. H., Wang, M. K., Lin, J. S., Zhao, G., and Ge, H. L. (2014). Effects of rainfall in tensity and slope gradient on steep colluvial deposit erosion in Southeast China. *Soil Sci. Soc. Am. J.* 78, 1741–1752. doi:10.2136/sssaj2014.04.0132

Jiang, J., Xu, R. K., and Zhao, A. Z. (2010). Comparison of the surface chemical properties of four soils derived from Quaternary red earth as related to soil evolution. *Catena* 80, 154–161. doi:10.1016/j.catena.2009.11.002

Li, H., Hou, J., Liu, X. M., Li, R., Zhu, H. L., and Wu, L. S. (2011). Combined determination of specific surface area and surface charge properties of charged particles from a single experiment. *Soil Sci. Soc. Am. J.* 75, 2128–2135. doi:10.2136/sssaj2010.0301

Lin, J., Huang, Y., Zhao, G., Jiang, F., Wang, M. K., and Ge, H. (2017). Flow-driven soil erosion processes and the size selectivity of eroded sediment on steep slopes using colluvial deposits in a permanent gully. *Catena* 157, 47–57. doi:10.1016/j.catena.2017.05.015

Ma, L., Wang, Q., and Yuan, G. H. (2007). Study on the microstructure of cementation function of free iron oxide in red soil. *J. Hebei Univ. Eng.* 24, 28–31. doi:10.3969/j.issn.1673-9469.2007.01.008

Mishra, P. N., Zhang, Y., Bhuyan, M. H., and Scheuermann, A. (2020). Anisotropy in volume change behaviour of soils during shrinkage. *Acta Geotech.* 15, 3399–3414. doi:10.1007/s11440-020-01015-6

Qafoku, N. P., and Sumner, M. E. (2002). Adsorption and desorption of indifferent ions in variable charge subsoils: the possible effect of particle interactions on the counter-ion charge density. *Soil Sci. Soc. Am. J.* 66, 1231–1239. doi:10.2136/sssaj2002.1231

Qafoku, N. P., Van Ranst, E., Noble, A., and Baert, G. (2004). Variable charge soils: their mineralogy, chemistry and management. *Adv. Agron.* 84, 159–215. doi:10.1016/S0065-2113(04)84004-5

Six, J., Bossuyt, H., Degryze, S., and Denef, K. (2004). A history of research on the link between (micro)aggregates, soil biota, and soil organic matter dynamics. *Soil till. Res.* 79, 7–31. doi:10.1016/j.still.2004.03.008

Wang, B., Zhang, G. H., Shi, Y. Y., and Zhang, X. C. (2014). Soil detachment by overland flow under different vegetation restoration models in the Loess Plateau of China. *Catena* 116, 51–59. doi:10.1016/j.catena.2013.12.010

Wang, B., Zhang, G. H., Yang, Y. F., Li, P. P., and Liu, J. X. (2018). The effects of varied soil properties induced by natural grassland succession on the process of soil detachment. *Catena* 166, 192–199. doi:10.1016/j.catena.2018.04.007

Wang, Y. P., Xu, R. K., and Li, J. Y. (2013). Effect of Fe/Al hydroxides on desorption of K+ and NH4+ from two soils and kaolinite. *Pedosphere* 1, 81–87. doi:10.1016/S1002-0160(12)60082-4

Wei, J., Shi, B., Li, J., Li, S., and He, X. (2018). Shear strength of purple soil bunds under different soil water contents and dry densities: a case study in the three gorges reservoir area, China. *Catena* 166, 124–133. doi:10.1016/j.catena.2018.03.021

Wu, X. L., Wei, Y. J., Wang, J. G., Wang, D., She, L., Wang, J., et al. (2017). Effects of soil physicochemical properties on aggregate stability along a weathering gradient. *Catena* 156, 205–215. doi:10.1016/j.catena.2017.04.017

Xia, J., Cai, C., Wei, Y., and Wu, X. (2019). Granite residual soil properties in collapsing gullies of south China: spatial variations and effects on collapsing gully erosion. *Catena* 174, 469–477. doi:10.1016/j.catena.2018.11.015

Xia, J., Cai, C., Wei, Y., Zhou, Y., Gu, J., Xiong, Y., et al. (2021). Variations of soil hydraulic properties along granitic slopes in Benggang erosion areas. *J. Soil. Sediment.* 21, 1177–1189. doi:10.1007/s11368-020-02843-5

Xu, J. X., and Zeng, G. H. (1992). "Benggang erosion in sub-tropical granite weathering crust geo-ecosystems: an example from Guangdong Province," in *Erosion, debris flows and environment in mountain regions*. Editor D. E. Walling, (Wallingford, Oxfordshire, UK: IAHS Publication), 455–463.

Xu, J. X. (1996). Benggang erosion: the influencing factors. *Catena* 27, 249–263. doi:10.1016/0341-8162(96)00014-8

Yu, T. R. (1997) *Chemistry of variable charge soils*. New York: Oxford University Press.

Zhang, X., and Kong, L. (2014). Interaction between iron oxide colloids and clay minerals and its effect on properties of clay. *Chin. J. Geotechnical Eng.* 36, 65–74. doi:10.11779/CJGE201401004

Zhang, Y., Zhao, D. F., Zheng, Q. M., Lin, J. S., Jiang, F. S., Huang, B. F., et al. (2022). Temperature on soil Atterberg limit in soil of collapsing gully wall in the hilly granitic region of south China. *Acta Pedol. Sin.* 59, 119–128. doi:10.11766/trxb20200730087

Zhang, Z., You, L. X., Lin, J. S., Wu, Y. B., Zhong, H. L., Chen, J., et al. (2023). Impact of soil surface properties on soil swelling of different soil layers in collapsing wall of Benggang. *Plos One* 18, e0280729. doi:10.1371/journal.pone.0280729

Zhong, B., Peng, S., Zhang, Q., Ma, H., and Cao, S. (2013). Using an ecological economics approach to support the restoration of collapsing gullies in southern China. *Land Use Policy* 32, 119–124. doi:10.1016/j.landusepol.2012.10.005